International Journal of Mass Spectrometry 278 (2008) 26–31

Contents lists available at ScienceDirect

International Journal of Mass Spectrometry

journal homepage: www.elsevier.com/locate/ijms

# The dissociation dynamics of energy-selected neopentylamine ions: Heats of formation of neopentylamine and neopentyl alcohol

Nicholas S. Shuman, James P. Kercher, Tomas Baer*

*The Department of Chemistry, The University of North Carolina at Chapel Hill, Chapel Hill, NC 27599-3290, United States*

ARTICLE INFO

*Article history:*
Received 6 June 2008
Received in revised form 23 July 2008
Accepted 24 July 2008
Available online 9 August 2008

*Keywords:*
Neopentyl amine
Photoionization
TPEPICO
Heat of formation

ABSTRACT

The dissociation dynamics of energy-selected neopentylamine cations, $(CH_3)_3CCH_2NH_2^+$, were studied using threshold photoelectron photoion coincidence (TPEPICO) spectroscopy in which ion time-of-flight (TOF) distributions are recorded as a function of the ion internal energy. The lowest energy pathway, producing the $CH_3NH_3^+$ ion, involves a rearrangement of the molecular ion. The 0 K dissociation onsets for the production of the $CH_3NH_3^+$, $CH_2NH_2^+$, and $(CH_3)_2CCH_2NH_2^+$ ions have been determined to be $9.54 \pm 0.05$, $9.647 \pm 0.025$ and $9.90 \pm 0.1$ eV, respectively. Because the heat of formation of the $CH_2NH_2^+ + t\text{-}C_4H_9^\bullet$ products are established, we can use the measured onset of 9.647 eV for this reaction to establish the neopentylamine $\Delta_f H^\circ_{298} = -130.3 \pm 3.3$ kJ/mol. This result is used in a group additivity scheme to estimate the neopentyl alcohol heat of formation as $\Delta_f H^\circ_{298} = -315.5 \pm 4$ kJ mol$^{-1}$. Both of these results are strongly supported by a series of isodesmic reactions calculated at the G3B3 and CBS-APNO levels. This is the first reported experimental heat of formation of the neopentylamine and the first reported heat of formation of the neopentyl alcohol.



## 1. Introduction

The $CH_2NH_2^+$ ion is the lowest energy fragment ion in the dissociative photoionization of small primary amines, $RCH_2NH_2$ where $R \leq C_4H_9$ [1–3]. Harvey and Traeger [2] and Traeger [3] took advantage of this property to determine an average heat of formation of the $CH_2NH_2^+$ ion from the dissociative photoionization of a series of primary amines. We recently measured the dissociation onsets for the $CH_2NH_2^+$ product ion for the same set of primary amines using threshold photoelectron photoion coincidence (TPEPICO) [1]. However, rather than assuming the heats of formation of the alkyl radicals, Bodi et al. [1] combined the experimental onset energies with calculated onsets from a network of isodesmic reactions to develop a self consistent set of alkyl radical and primary amine heats of formation with error limits of 2 kJ/mol.

The addition of an extra $CH_2$ group to the alkyl chain, generates amines that can dissociatively ionize to produce the methylenimmonium ion and the *n*-butyl, *iso*-butyl, or *t*-butyl radicals. However, this reaction is now in competition with other dissociation paths, making the $C_4H_9CH_2NH_2^+$ ion dissociation dynamics more difficult to interpret. Among these is neopentylamine, which dissociates to several products, including $CH_2NH_2^+ + t\text{-}C_4H_9^\bullet$. We have recently developed modeling schemes that permit us to quantitatively interpret higher energy thresholds for parallel and consecutive reaction paths [4], and we use this approach here to interpret the neopentylamine TPEPICO data.

## 2. Experimental

The TPEPICO apparatus has been described in detail elsewhere [5,6], thus only a brief summary is given here. Sample vapor at a controlled temperature between 210 and 400 K is introduced into the ionization region through a small stainless steel capillary and ionized with vacuum ultraviolet (VUV) light from a hydrogen discharge lamp dispersed by a 1 m normal incidence monochromator with a resolution of 8 meV at a photon energy of 10.0 eV. The VUV wavelengths are calibrated by using the Lyman-α emission at 1215.67 Å, which is the most intense line in this spectrum. The ions and electrons are extracted in opposite directions with an electric field of 20 V/cm. Electrons pass through a second acceleration region where they are accelerated to a final energy of 74 eV. They then drift 13 cm along a field free drift region. The applied voltages are designed to velocity focus threshold electrons onto a 1.4 mm aperture at the end of the electron drift region, where a channeltron detects them. At the same time energetic electrons are focused to concentric rings around the central hole, the diameter of which is dependant on their initial perpendicular velocity component. Electrons hitting a $3 \times 7$ mm opening centered 5 mm away from the

* Corresponding author. Tel.: +1 919 962 1580; fax: +1 919 962 2388.
*E-mail address:* baer@unc.edu (T. Baer).

1387-3806/$ – see front matter © 2008 Elsevier B.V. All rights reserved.
doi:10.1016/j.ijms.2008.07.036

central hole are collected by a second channeltron and provide a measure of the hot electron signal. By subtracting a fraction of the coincidence spectrum obtained with the second channeltron from the TPEPICO spectrum, we obtain a TPEPICO spectrum free of 'hot' electron contamination.

Ion time-of-flights (TOF) are determined with one of two ion optics arrangements. In the linear time-of-flight mass spectrometer (LinTOF), ions are accelerated first to 100 eV in a 4.8 cm acceleration region and then to 260 eV in a second 0.2 cm region. The ions pass through a 26 cm drift region and are then decelerated to 210 eV, where they drift for another 7.6 cm before being collected by a chevron multichannel plate detector. In the reflecting time-of-flight mass spectrometer (ReTOF), the ions are accelerated to 100 eV in the first 5 cm long acceleration region and travel 40 cm in the first drift region. Ions are then reflected and travel through another 35 cm second drift region before being collected by a tandem multichannel plate ion detector. The electron and ion signals are used as start and stop pulses for measuring the ion time-of-flight (TOF). TPEPICO TOF spectra with good signal to noise were collected in 2–12 h. The TOF distributions, obtained at series of closely spaced photon energy, are used to obtain the fractional abundance of the precursor and the product ions (breakdown diagram).

If the dissociation is rapid, the fragment TOF peaks are symmetric. A reverse barrier in the dissociation channel, which is associated with significant translational energy release, appears as a peak broadening. On the other hand, a slow reaction, taking place on the time scale of microseconds, results in an asymmetric TOF peak because the ions are dissociating while accelerating in the 5 cm long acceleration region.

## 3. Results and discussion

Time-of-flight mass spectra were obtained at a range of energies between 9.0 and 12.0 eV at both room temperature and at 223 K. Typical TOF distributions obtained at several photon energies are shown in Fig. 1. These spectra have been corrected for the presence of energetic electrons. The peak at 21.3 μs corresponds to the neopentylamine ion, the peak at 19.2 μs is the $(CH_3)_2CCH_2NH_2^+$ ion, resulting from the methyl loss channel, and the $CH_2NH_2^+$ ion is observed at 12.5 μs. The asymmetric peak from 12.8 to 17.5 μs corresponds to the $CH_3NH_3^+$ ion. The asymmetry of the TOF peak arises from ions that dissociate slowly and therefore do so across a range of positions throughout the acceleration region. The peak at

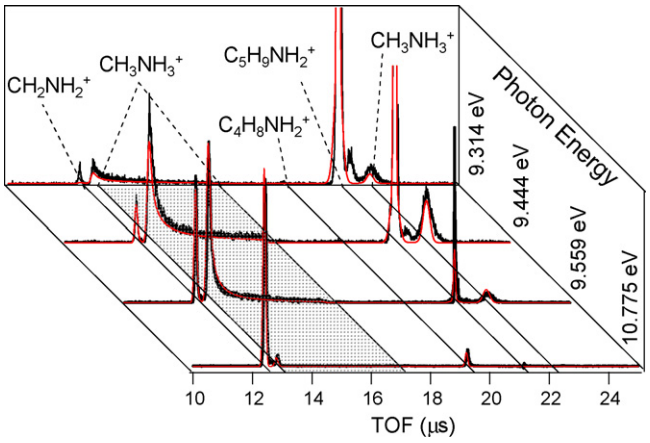


**Fig. 1.** TOF mass spectra at the photon energies indicated collected at 223 K on the LinTOF mass spectrometer (see text). Black lines are experimental points, red lines are best-fit RRKM simulations using model 2 (see text). (For interpretation of the references to color in this figure legend, the reader is referred to the web version of the article.)

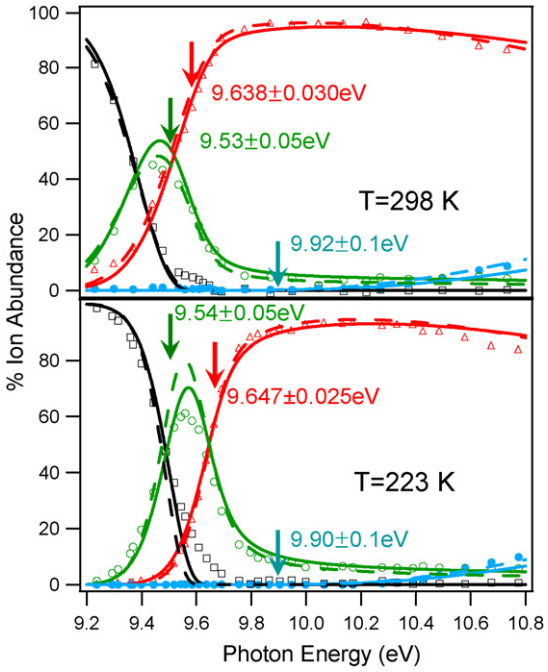


**Fig. 2.** Breakdown diagrams of the dissociation of $t$-$C_4H_9CH_2NH_2^+$ at room temperature and at 223 K. Points are measured ion abundances for $(CH_3)_3CH_2NH_2^+$ (open squares, black), $CH_2NH_2^+$ (open triangles, red), $CH_3NH_3^+$ (open circles, green), and $(CH_3)_2CH_2NH_2^+$ (closed circles, blue). Lines are best-fit RRKM curves from model 1 (dashed, see text) and model 2 (solid, see text). Average dissociation onsets from the two models are shown, individual values appear in Table 1. (For interpretation of the references to color in this figure legend, the reader is referred to the web version of the article.)

22.2 μs is attributed to $CH_3NH_3^+$ ions produced in the drift region (ions which dissociate in the drift region appear at TOF's longer than that of the parent ion due to the subsequent deceleration region), allowing for one extra data point in the determination of the rate constant of that channel at each photon energy.

The fractional abundance, corrected for the hot electron contamination, of all ions from the recorded TOF spectra at many different photon energies are plotted as a function of the photon energy, yielding the breakdown curves given in Fig. 2. The open points are the experimentally determined ion ratios and the solid lines are the simulated ion ratios. At low energy, only the neopentylamine ion, $(CH_3)_3CCH_2NH_2^+$, is present. At higher energies the $CH_3NH_3^+$ ion is observed, but it is quickly overtaken by the appearance of the $CH_2NH_2^+$ ion. Above 10 eV, a $CH_3^\bullet$ loss channel for the production of the $(CH_3)_2CCH_2NH_2^+$ ion opens up. The reaction scheme is summarized in Eqs. (1a)–(1c).

$$\begin{aligned} & \rightarrow CH_3NH_3^+ + CH_3CCH_2CH_2^\bullet \quad (a) \\ (CH_3)_3CCH_2NH_2 + h\nu \ & \rightarrow CH_2NH_2^+ + C(CH_3)_3^\bullet \quad (b) \\ & \rightarrow (CH_3)_2CCH_2NH_2^+ + CH_3^\bullet \quad (c) \end{aligned} \tag{1}$$

The asymmetric TOF distributions in Fig. 1 for the lowest energy reaction (1a) leading to the $CH_3NH_3^+$ ion, permit us to measure the dissociation rate constants, $k(E)$, for this rearrangement reaction. As a result, the relative rates for reactions (1b) and (1c) can be placed on an absolute basis at higher energies, where their peaks are just barely asymmetric. The derived rate curves are shown in Fig. 3.

### 3.1. Modeling parallel dissociation pathways

Low-energy ions of the primary amines $RNH_2$ (R = $CH_3$, $C_2H_5$, $C_3H_7$, $C_4H_9$, $i$-$C_4H_9$) dissociate exclusively by cleavage at the α-carbon to produce $CH_2NH_2^+$. The neopentylamine ion, however,

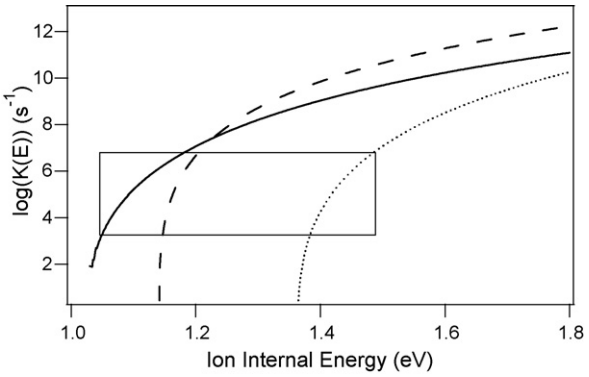


**Fig. 3.** Rate constants determined from RRKM modeling of observed TOF spectra for channels 1a (solid line), 1b (dashed line), and 1c (dotted line) (see text). The overlayed box indicates the range over which direct rate information is measured.

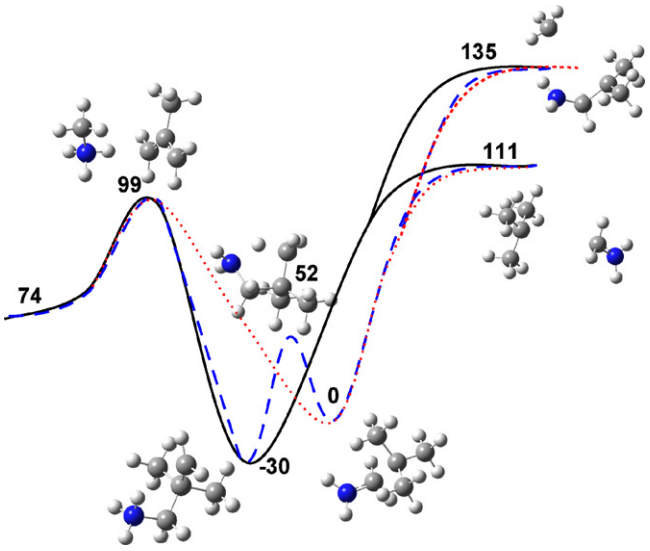


**Fig. 4.** Reaction coordinates of models 1 (dotted, red), 2 (solid, black), and 3 (dashed, blue) (see text for description of each model) and best-fit dissociation barrier heights (kJ mol$^{-1}$) relative to the neopentylamine ion. Structures shown are either stationary points or, for dissociating species, results of constrained optimizations at the B3LYP/6-31G* level. (For interpretation of the references to color in this figure legend, the reader is referred to the web version of the article.)

fragments via several parallel, competing pathways in the energy range from 9.0 to 12.0 eV. The modeling of parallel pathways has been published in detail previously [4], and we follow the same approach here. This is done by taking into account the neopentylamine thermal energy distribution, which is determined from the DFT calculated vibrational and rotational frequencies of the neutral molecule. The rate constants for the three reactions (1a)–(1c) were calculated by RRKM theory [7] using calculated vibrational frequencies of the dissociating ion and its transition states. The transition state frequencies for simple bond cleavage reactions were obtained by stretching the bond that breaks to about 4 Å and calculating the frequencies for this extended structure. The one imaginary frequency is the bond stretch. The five lowest real frequencies (assumed to correspond to the five vibrational modes transitioning into product rotations) along with the dissociation onset energies are treated as optimizable parameters in order to obtain a best-fit to both the breakdown diagram and TOF spectra.

The results of the modeling obviously depend on the nature of the dissociating ion and the transition states to each product. This presents a problem because we do not know the mechanism for the $CH_3NH_3^+$ production, which involves the transfer of two hydrogen atoms, nor do we understand why this product is observed in the neopentylamine ion dissociation but not in the dissociation of other primary amine ions. The latter point is particularly interesting because this channel produces more stable products than does α-cleavage in the cases of not only the neopentyl but also the *n*-butyl and isobutyl amine ions. Bowen and Williams [8] and Bowen and Maccoll [9] noted that isobutyl alcohol ions dissociate primarily to $CH_3OH_2^+$ (analogous to channel 1a) while isobutylamine ions dissociate primarily to $CH_2NH_2^+$ (analogous to channel 1b). They proposed that in both cases as the α C–C bond is stretched an intermediate complex (e.g., [propene + methanol]$^{\bullet+}$ for isobutyl alcohol) is stabilized by ion-dipole attractions, allowing for a molecular rearrangement and double-hydrogen transfer in the case of the alcohol but not the amine due to a proposed low-energy alkene–alcohol ion complex, but a somewhat higher energy alkene–amine ion complex. The strong long-range attraction in the mechanism would suggest a late, loose transition state.

Hammerum and Derrick [10] rejected this argument by noting that low-energy neopentylamine ions dissociate primarily to $CH_3NH_3^+$ while isobutylamine ions do not, and that the respective alkene–amine ion complexes would have very similar heats relative to the respective ground state ions. Hammerum suggests an alternative mechanism elucidated from the behavior of selectively deuterated amines. Mass spectra of $RND_2$ (R = propyl, isobutyl, butyl, neopentyl) ionized by 70 eV electrons show significant scrambling in both $CH_2NH(D)_2^+$ and $CH_3NH(D)_3^+$ production, whereas deuteration of the α-carbon in isobutyl and neopentyl amine shows no scrambling. This suggests that in the cases of both isobutyl and neopentyl amine ions, a reversible 1,4 hydrogen transfer readily occurs (whether or not the eventual dissociation is to $CH_3NH_3^+$) and the $CH_3NH_3^+$ channel must involve a second hydrogen transfer to the α-carbon.

The ill-defined and complicated mechanism for channel 1a presents a challenge to model and for the accurate extraction of a dissociation onset. On the other hand, the goal of this work, the determination of the neopentylamine heat of formation, depends only on the onset of channel 1b. If the rate of channel 1a is accurately reproduced over the experimental range, regardless of the correctness of the mechanism, the onset of channel 1b can be determined. To this end, we attempt to model the dissociation by the simplest method possible that reproduces the measured rates for channel 1a.

First, we treat all three dissociations as simple bond cleavages of the neopentylamine ion. This model cannot reproduce the rates of channel 1a across the full experimental range. The data can be fit, however, by assuming a reverse barrier in channel 1a (Fig. 4, model 1). The heats of formation for the products of both channels 1a and 1b are fairly well established [1,11–14], so that we can fix the difference between the final product energies at 37 kJ mol$^{-1}$. By varying the height of the reverse barrier and the critical imaginary frequency of the transition state (tunneling is modeled by assuming an Eckart barrier [7]) we obtain a good fit to the data assuming a critical frequency of 700*i* cm$^{-1}$. We are unclear on the nature of the transition state of channel 1a and treat the lowest calculated frequencies of $[CH_3NH_3\cdots t\text{-}C_4H_9]^+$ as adjustable parameters to fit the experimentally determined dissociation rates. The fits to the breakdown diagrams appear in Fig. 2, and the best-fit dissociation onsets and activation entropies appear in Table 1. The best-fit TOF spectra are nearly identical to those presented in Fig. 1. Uncertainties are determined for each onset by fixing that onset to values higher or lower than the determined best-fit until no reoptimization produces a good fit to the experimental data, as judged by eye.

**Table 1**
Best-fit dissociation onsets and activation entropies at 600 K for $t$-$C_4H_9CH_2NH_2^+$ dissociation at 223 K

| | Channel 1a[a] | | Channel 1b[a] | | Channel 1c[a] | |
|---|---|---|---|---|---|---|
| | $E_0$ (eV) | $\Delta S^{\#}$ (J mol$^{-1}$ K$^{-1}$) | $E_0$ (eV) | $\Delta S^{\#}$ (J mol$^{-1}$ K$^{-1}$) | $E_0$ (eV) | $\Delta S^{\#}$ (J mol$^{-1}$ K$^{-1}$) |
| Model 1[a] | | | | | | |
| 223 K | 9.55 ± 0.05 | 96 | 9.650 ± 0.025 | 133 | 9.90 ± 0.1 | 151 |
| 298 K | 9.53 ± 0.05 | 96 | 9.638 ± 0.030 | 133 | 9.94 ± 0.1 | 151 |
| Model 2[a] | | | | | | |
| 223 K | 9.52 ± 0.05 | 120 | 9.644 ± 0.025 | 152 | 9.90 ± 0.1 | 163 |
| 298 K | 9.53 ± 0.05 | 120 | 9.638 ± 0.030 | 152 | 9.90 ± 0.1 | 163 |

[a] See text for model and channel descriptions.

Although model 1 (with the exit barrier) accurately models the rate of $CH_3NH_3^+$ production, channel 1a cannot be the result of a simple bond cleavage from neopentylamine ion, and the mechanism likely proceeds through the distonic ion produced by 1,4 hydrogen transfer. We can model the dissociation as described above, but with all products leaving instead from this isomer (Fig. 4, model 2). The best-fit TOF spectra and breakdown diagrams are shown in Figs. 1 and 2. Best-fit parameters appear in Table 1. Both mechanisms produce nearly identical dissociation onsets for all three channels. Model 2 does not explicitly consider isomerization between the neopentylamine ion and the distonic isomer. If, however, we assumed the isomerization to be fast and the populations in equilibrium, the dissociation rate would be a function of the sum of the densities of states of two ions [7]. Because the distonic ion isomer is significantly lower in energy, its density of states would be much larger and dominate that sum, and the calculated dissociation rates would be approximately the same as those derived from model 2.

By finding the isomerization transition state using the QST2 method, we calculate the forward and reverse barriers by the G3B3 method to be 53 and 83 kJ mol$^{-1}$, respectively. These calculated barrier heights are similar to those calculated for 1,4 hydrogen transfer occurring in other primary amines [15,16]. However, by modeling the dissociation assuming this isomerization barrier (Fig. 4, model 3), we are unable to fit our data. In particular, the constant 5% abundance of $CH_3NH_3^+$ observed at photon energies above 10 eV indicates that the rate curves of channels 1a and 1b are parallel, and we can only reproduce this feature if the isomerization occurs much faster than that suggested by the calculations. Our data are consistent with a negligibly small barrier to the 1,4 hydrogen transfer isomerization. It is not apparent if this discrepancy extends to other primary amines which do not dissociate to $CH_3NH_3^+$ and therefore lack the same means of comparison between the experiment and calculations.

Finally, it is important to note that the best-fit onset to channel 1b (the only one from which we extract thermochemical data) was identical to within 0.9 kJ mol$^{-1}$, regardless of the mechanism used to model the $CH_3NH_3^+$ dissociation. Additionally, while the literature value of the ionization energy of neopentylamine [17] has a relatively large (8.5 ± 0.1 eV) uncertainty, the value calculated by the G3B3 method, 8.53 eV, agrees very well, and in any case the best-fit onset for channel 1b was insensitive to the value used.

### 3.2. The neopentylamine heat of formation

The 0 K onset for the $NH_2CH_2^+ + C_4H_9^\bullet$ channel can be used to establish the heat of formation of the neopentylamine because both the methylenimmonium ion [1–3] and the $t$-butyl radical [13,18] have well established heats of formation (see Table 1). Because the dissociation onset of neopentylamine at 223 K is sharper than at room temperature, we consider the colder values more reliable and use the average onset at this temperature from models 1 and 2 described above. This leads to a 0 K neopentylamine heat of formation of −90.4 ± 3.3 kJ mol$^{-1}$, which can be converted to a 298 K heat of formation of −130.3 kJ mol$^{-1}$ by the usual thermochemical cycle using vibrational frequencies calculated at the B3LYP/6-311++G** level. No value for this molecule is found in the most recent Pedley compilation [19] or a search of more recent literature. However, the estimation method of Pedley [19], which provides excellent agreement with experimental heats of formation of other primary alkanes (Table 2), suggests a 298 K heat of formation of 129.1 kJ mol$^{-1}$, in agreement with our experiment. Additionally, a value of −130 kJ mol$^{-1}$ was extracted by Hammerum from the proton affinities of a series of amines [17] by an undocumented method and without a reported uncertainty [10].

We can evaluate the accuracy of the experimental heat through high level ab initio calculations. Bodi et al. [1] determined the heats of formation of a series of primary amines ($RNH_2$: R = $CH_3$, $C_2H_5$, $C_3H_7$, $C_4H_9$, $i$-$C_4H_9$) by linking two isodesmic reaction networks through the experimentally determined 0 K onsets of dissociations analogous to channel 1b. The heats of formation of the amines, methylenimmonium ion, and alkyl radical co-products were optimized to minimize discrepancies between calculated and experimental values throughout the network. Here we expand the reaction networks

$$RNH_2 + R'CH_3 \rightarrow RCH_3 + R'NH_2$$

$$R^\bullet + R'CH_3 \rightarrow RCH_3 + R'^\bullet$$

to include neopentylamine and the $t$-butyl radical. The average 0 K heat of formation of neopentylamine determined from five isodesmic reactions

$$C_4H_9CH_2NH_2 + RCH_3 \rightarrow C_4H_9CH_2CH_3 + RNH_2 (R = CH_3, C_2H_5, C_3H_7, C_4H_9, i\text{-}C_4H_9)$$

**Table 2**
Comparison of experimental and estimated heats of formation

| | $\Delta H^\circ_{f,298\ K}$ (kJ mol$^{-1}$) | |
|---|---|---|
| | Experiment | Pedley method[a] |
| $CH_3NH_2$ | −21.8 ± 1.5[b] | −23.5 |
| $C_2H_5NH_2$ | −50.1 ± 1.5[b] | −49.9 |
| $C_3H_7NH_2$ | −70.8 ± 1.5[b] | −70.7 |
| $C_4H_9NH_2$ | −89.6 ± 2.0[b] | −91.5 |
| $i$-$C_4H_9NH_2$ | −97.8 ± 1.0[b] | −98.2 |
| $t$-$C_4H_9CH_2NH_2$ | −130.3 ± 3.3[c] | −129.1 |
| $t$-$C_4H_9CH_2OH$ | −315.4 ± 4[d] | −314.3 |

[a] From Ref. [19].
[b] From Ref. [1].
[c] Derived from this experiment.
[d] Value estimated from $t$-$C_4H_9CH_2NH_2$ and $t$-$C_4H_9CH_2CH_3$ heats as described in the text.

**Table 3**
New heats of formation resulting from this work and ancillary values used (kJ mol$^{-1}$)

| Species | $\Delta_f H^\circ_0$ | | $\Delta_f H^\circ_{298}$ | $H_{298} - H_0$ |
|---|---|---|---|---|
| | Experiment | Calculated[a] | | |
| $NH_2CH_2^+$ | | | 750.3 ± 1.0[b] | 10.4 |
| *t*-$C_4H_9$• | 76.4 ± 2.0[c] | 77.2 ± 4 | 51.8 ± 2.0[c] | 17.7 |
| *t*-$C_4H_9CH_2NH_2$ | −90.4 ± 3.3 | −92.0 ± 4 | −130.3 ± 3.3 | 24.7[d] |
| *t*-$C_4H_9CH_2OH$ | −279.3 ± 4[e] | −282.3 ± 4 | −315.5 ± 4[e] | 24.2[d] |

[a] Average value of isodesmic reaction described in the text at the G3B3 and CBS-APNO levels.
[b] From Bodi et al. [1].
[c] Average of Berkowitz et al. [14] and Traeger [13].
[d] Heats of formation are converted between 0 and 298 K by the standard thermochemical cycle using harmonic vibrational frequencies calculated using Gaussian 03 at the B3LYP/6-311++G** level. Treatment of internal rotations as vibrations slightly underestimates the correction to the thermal enthalpy. Adjustments of 0.8 kJ mol$^{-1}$ for neopentylamine and 0.65 kJ mol$^{-1}$ for neopentyl alcohol are estimated from the corrections explicitly calculated for a series of other primary amines and alcohols [1].
[e] Value estimated from *t*-$C_4H_9CH_2NH_2$ and *t*-$C_4H_9CH_2CH_3$ heats as described in the text.

using the Gaussian 03 quantum chemical package [20] (G3B3 and CBS-APNO levels) is −92.0 ± 4 kJ mol$^{-1}$. The results of these calculations as well as auxiliary literature heats of formation used are available as online supporting information. Assigning reliable uncertainties to the results of the isodesmic calculations requires some estimation. The CBS-APNO [21] and G3B3 [22] methods have been shown to calculate energies with mean absolute deviations of within 4 kJ mol$^{-1}$ for both closed and open-shell [23] species, and we assume this as the uncertainty in each individual calculated energy. Convoluting the four calculated energies involved in the determination of each heat of reaction yields an uncertainty of 8 kJ mol$^{-1}$, and combining the results of the two-independent methods used for each reaction yields an uncertainty of 5.7 kJ mol$^{-1}$ for each of the five isodesmic heat of reactions. We consider these errors to be conservative because we do not take into account the cancellation of errors associated with the use of isodesmic reaction energies. This error convoluted with the uncertainties of the literature values $RCH_3$, $RNH_2$, and 2,2-dimethyl butane yields the uncertainty in each derived heat of formation of neopentylamine. Because the literature values are all known quite precisely, the uncertainty in the calculation dominates and we report the heat of formation uncertainties as 6 kJ mol$^{-1}$. The neopentylamine heats of formation derived from the five isodesmic reactions are not entirely independent of one another (they each depend on the calculated values of neopentylamine and 2,2-dimethyl butane) and cannot be trivially combined, however a sum uncertainty of 4 kJ mol$^{-1}$ in the calculated 0 K neopentylamine heat of formation is reasonable. We note that all five values lie within 1.2 kJ mol$^{-1}$ of the mean.

The calculated heat of formation is in excellent agreement with our experimental value (−90.4 ± 3.3 kJ mol$^{-1}$). Furthermore, the average calculated 0 K heat of formation of the *t*-butyl radical, derived from the second set of isodesmic reactions, is 77.2 ± 4 kJ mol$^{-1}$, which is in good agreement with the recommendation of Berkowitz, Ellison, and Gutman and the recent determination by Traeger [13,14]. The two series of isodesmic reactions are linked by the onset of channel 1b. Because the average calculated $E_0$ (9.663 eV ± 0.05) is in good agreement with our experimentally determined onset (9.647 ± 0.025 eV), the reaction network remains self-consistent without reoptimization of the other amine or radical heats. Experimental and calculated heats of formation are summarized in Table 3.

It is interesting to note that up until 1994, there was significant debate about the heat of formation of the *t*-butyl radical. The value measured by Seakins et al. [24] and recommended by Berkowitz et al. [14] is more positive than most previous determinations but has gained general acceptance due to subsequent theoretical [25] and experimental [13,26,27] verification. The inclusion of the *t*-butyl radical and the channel 1b onset into the self-consistent isodesmic reaction network also supports this so-called "high" value of the *t*-butyl radical heat of formation.

### 3.3. Estimate of the neopentyl alcohol heat of formation

Not only does the Pedley [19] compilation not include neopentylamine, the neopentyl alcohol heat of formation is listed only for the liquid phase and with an error of ±16.7 kJ mol$^{-1}$. On the other hand, the hydrocarbon analog, 2,2-dimethyl butane is listed with a gas phase heat of formation of −185.9 ± 0.9 kJ mol$^{-1}$. We can use these values to estimate a better value for the neopentyl alcohol heat of formation by noting the trends in the heats of formation for a series of alkanes, amines, and alcohols shown in Table 4. If we simply subtract the difference in the heats of formation between the primary alcohols and the amines for ethyl, *n*-propyl, *n*-butyl, and *iso*-butyl analogues, we obtain a difference of 185.2 ± 1.1 kJ mol$^{-1}$. Similarly, the difference between the alcohols and the alkanes are 129.5 ± 0.8 kJ mol$^{-1}$. That is, the differences are essentially constant. In principle, we should be able to extrapolate this pattern to obtain a much more accurate value for the neopentyl

**Table 4**
298 K heats of formation of primary alkanes, amines, and alcohols (kJ mol$^{-1}$)

| R–X | X = $CH_3$[a] | X = $NH_2$[b] | X = OH | Δ($CH_3$–OH)[c] | Δ($NH_2$–OH)[d] |
|---|---|---|---|---|---|
| $C_2H_5X$ | −104.7 ± 0.5 | −50.1 ± 1.5 | −235.2 ± 0.3[a] | 130.5 | 185.1 |
| *n*-$C_3H_7X$ | −125.7 ± 0.6 | −70.8 ± 1.5 | −255.1 ± 0.4[a] | 129.4 | 184.3 |
| *n*-$C_4H_9X$ | −146.9 ± 0.8 | −89.6 ± 2.0 | −274.9 ± 0.5[a] | 128.0 | 185.3 |
| *i*-$C_4H_9X$ | −153.6 ± 0.9 | −97.8 ± 1.0 | −283.8 ± 0.8[a] | 130.2 | 186.0 |
| | | | | 129.5 (ave) | 185.2 (ave) |
| $CH_3C(CH_3)_2CH_2X$ | −185.9 ± 0.9 | −130.3 ± 3.3[e] | −315.5 ± 4[f] | 129.4 | 185.2 |

[a] From Pedley [19].
[b] From Bodi et al. [1].
[c] Difference between columns 2 and 4.
[d] Difference between columns 3 and 4.
[e] Determined in this study.
[f] Estimated by using the average differences between the corresponding alkane and alcohol and amine and alcohol heats of formation.

alcohol heat of formation. If we use the literature 298 K heat of formation of 2,2-dimethyl butane of $-185.9 \pm 0.9$ kJ mol$^{-1}$ [19], and subtract 129.5, we obtain a neopentyl alcohol heat of formation of $-315.4$ kJ mol$^{-1}$. If we begin with the neopentyl amine heat of formation of $-130.3 \pm 3.3$ kJ mol$^{-1}$ determined in this study and subtract 185.2, we obtain $-315.5$ kJ mol$^{-1}$, in excellent agreement with the extrapolation from the alkane. The Pedley method [19] (see Table 2) produces a similar value of $-314.3$ kJ mol$^{-1}$.

Although the simplicity of group additivity is appealing, and in this particular case the method is fairly convincing, the lack of a 'hard' experimental result naturally lends increased uncertainty to the determination. We can use high level ab initio calculations to help support or refute the estimated value. The average heat of formation determined in a similar manner to that of neopentyl amine described above by two series of isodesmic reactions:

$$C_5H_{11}OH + RCH_3 \rightarrow ROH + C_5H_{11}CH_3$$

$$C_5H_{11}OH + RNH_2 \rightarrow ROH + C_5H_{11}NH_2$$

calculated at the G3B3 and CBS-APNO levels (calculated energies are available as online supplemental information) agrees well with the group additivity results, yielding a slightly more negative 298 K heat of formation of $-318.5 \pm 4$ kJ mol$^{-1}$. Our suggested heat of formation based on the group additivity scheme appears in Table 1.

## 4. Summary

TPEPICO spectroscopy can provide a wealth of kinetic and energetic information. Even in the case of the neopentylamine ion dissociation which occurs through multiple competing pathways, the mechanisms of which are in part unclear, the absolute rates of the dissociations are well enough determined by the experiment that accurate dissociation onsets can be determined through RRKM modeling. Combined with previously determined values, the onset of $(CH_3)_3CCH_2NH_2 \rightarrow CH_2NH_2^+ + (CH_3)_3C^\bullet$ yields the heat of formation of neopentylamine, and this value is used to estimate the heat of formation of neopentyl alcohol. Both of these results are strongly supported by excellent agreement with heats of formation calculated by a series of isodesmic reactions.

## Acknowledgements

We gratefully acknowledge the financial support of a US Department of Energy grant. We also thank Prof. Bálint Sztáray for help in modeling the competitive decay mechanism and three excellent reviewers whose suggestions greatly improved our analyses.

## Appendix A. Supplementary data

Supplementary data associated with this article can be found, in the online version, at doi:10.1016/j.ijms.2008.07.036.

## References

[1] A. Bodi, J.P. Kercher, C. Bond, P. Meteesatien, B. Sztáray, T. Baer, J. Phys. Chem. A 110 (2006) 13425.
[2] Z.A. Harvey, J.C. Traeger, Eur. J. Mass Spectrom. 10 (2004) 759.
[3] J.C. Traeger, J. Phys. Chem. A 111 (2007) 4643.
[4] T. Baer, B. Sztáray, J.P. Kercher, A.F. Lago, A. Bodi, C. Scull, D. Palathinkal, Phys. Chem. Chem. Phys. 7 (2005) 1507.
[5] B. Sztaray, T. Baer, Rev. Sci. Instrum. 74 (2003) 3763.
[6] A.F. Lago, J.P. Kercher, A. Bodi, B. Sztaray, B. Miller, D. Wurzelmann, T. Baer, J. Phys. Chem. A 109 (2005) 1802.
[7] T. Baer, W.L. Hase, Unimolecular Reaction Dynamics: Theory and Experiments, Oxford University Press, New York, 1996.
[8] R.D. Bowen, D.H. Williams, J. Chem. Soc.-Chem. Commun. (1981) 836.
[9] R.D. Bowen, A. Maccoll, J. Chem. Soc.-Perkin Trans. 2 (1984) 1005.
[10] S. Hammerum, P.J. Derrick, J. Chem. Soc.-Perkin Trans. 2 (1986) 1577.
[11] E.P.L. Hunter, S.G. Lias, J. Phys. Chem. Ref. Data 27 (1998) 413.
[12] K.C. Lau, W.X. Zheng, N.B. Wong, J. Chem. Phys. 127 (2007).
[13] J.C. Traeger, J. Phys. Chem. A 112 (2008) 342–346.
[14] J. Berkowitz, G.B. Ellison, D. Gutman, J. Phys. Chem. 98 (1994) 2744.
[15] B.F. Yates, L. Radom, J. Am. Chem. Soc. 109 (1987) 2910.
[16] S. Hammerum, C.B. Nielsen, J. Phys. Chem. A 109 (2005) 12046.
[17] D.H. Aue, H.M. Web, M.T. Bowers, J. Am. Chem. Soc. 98 (1976) 311.
[18] A. Bodi, J.P. Kercher, C. Bond, P. Meteesatien, B. Sztaray, T. Baer, J. Phys. Chem. A 110 (2006) 13425.
[19] J.B. Pedley, Thermochemical Data and Structures of Organic Compounds, Thermodynamics Research Center, College Station, 1994.
[20] M.J. Frisch, G.W. Trucks, H.B. Schlegel, G.E. Scuseria, M.A. Robb, J.R. Cheeseman, J.A. Montgomery, T. Vreven, K.N. Kudin, J.C. Burant, J.M. Millam, S.S. Iyengar, J. Tomasi, V. Barone, B. Mennucci, M. Cossi, G. Scalmani, N. Rega, G.A. Petersson, H. Nakatsuji, M. Hada, M. Ehara, K. Toyota, R. Fukuda, J. Hasegawa, M. Ishida, T. Nakajima, Y. Honda, O. Kitao, H. Nakai, M. Klene, X. Li, J.E. Knox, H.P. Hratchian, J.B. Cross, C. Adamo, J. Jaramillo, R. Gomperts, F. Stratmann, O. Yazyev, A.J. Austin, R. Cammi, C. Pomelli, J.W. Ochterski, P.Y. Ayala, K. Morokuma, G.A. Voth, P. Salvador, J.J. Dannenberg, V.G. Zakrzewski, S. Dapprich, A.D. Daniels, M.C. Strain, Ö. Farkas, D.K. Malick, A.D. Rabuck, K. Raghavachari, J.B. Foresman, J.V. Ortiz, Q. Cui, A.G. Baboul, S. Clifford, J. Cioslowski, B.B. Stefanov, G. Liu, A. Liashenko, P. Piskorz, I. Komáromi, R.L. Martin, D.J. Fox, T. Keith, M.A. Al-Laham, C.Y. Peng, A. Nanayakkara, M. Challacombe, P.M.W. Gill, B. Johnson, W. Chen, M.W. Wong, C. Gonzalez, J.A. Pople, Gaussian 03, Revision C.02. Gaussian Inc.: Wallingford, CT, 2004.
[21] J.W. Ochterski, G.A. Petersson, J.A. Montgomery, J. Chem. Phys 104 (1996) 2598.
[22] A.G. Baboul, L.A. Curtiss, P.C. Redfern, K. Raghavachari, J. Chem. Phys. 110 (1999) 7650.
[23] D.J. Henry, C.J. Parkinson, L. Radom, J. Phys. Chem. A 106 (2002) 7927.
[24] P.W. Seakins, M.J. Pilling, J.T. Niiranen, D. Gutman, L.N. Krasnoperov, J. Phys. Chem. 96 (1992) 9847.
[25] B.J. Smith, L. Radom, J. Phys. Chem. A 102 (1998) 10787.
[26] N.K. Srinivasan, J.H. Kiefer, R.S. Tranter, J. Phys. Chem. A 107 (2003) 1532.
[27] J.A. Seetula, I.R. Slagle, J. Chem. Soc.-Faraday Trans. 93 (1997) 1709.